Analysis of *L*-shell line spectra with 50-ps time resolution from Mo *X*-pinch plasmas

S. B. Hansen and A. S. Shlyaptseva
Physics Department/220, University of Nevada, Reno, Nevada 89557, USA

S. A. Pikuz and T. A. Shelkovenko
Laboratory of Plasma Studies, 369 Upson Hall, Cornell University, Ithaca, New York 14853, USA
and P. N. Lebedev Physical Institute, Leninskii Pr. 53, Moscow, 119991, Russia

D. B. Sinars
Laboratory of Plasma Studies, 369 Upson Hall, Cornell University, Ithaca, New York 14853, USA
and Sandia National Laboratories, P.O. Box 5800, Albuquerque, New Mexico 87185-1193, USA

K. M. Chandler and D. A. Hammer
Laboratory of Plasma Studies, 369 Upson Hall, Cornell University, Ithaca, New York 14853, USA
(Received 23 January 2004; published 10 August 2004)

Mo wire *X* pinches typically emit several x-ray bursts from a bright spot near the crossing of the *X*-pinch wires. Streak camera images of *L*-shell line emission from Mo wire *X* pinches have been analyzed using a non-local thermodynamic equilibrium (NLTE) collisional-radiative atomic kinetics model, providing temperature and density profiles with ~50 ps time resolution over the ~350 ps x-ray bursts. In conjunction with nonspectroscopic measurements, the analysis is used to propose a picture of the dynamic evolution of the *X*-pinch plasma. The *L*-shell spectra from the first x-ray burst indicate an electron density near 10^{22} cm^{-3} and an electron temperature near 1 keV; subsequent x-ray bursts have *L*-shell spectra that indicate electron temperatures slightly above 1 keV and electron densities near 10^{20} and 10^{21} cm^{-3}. The size of the *L*-shell line-emitting region is estimated to be near 10 μm for the first x-ray burst and much larger for the later bursts. It is proposed that inner-shell excitation of low ionization stages of Mo in a μm-scale plasma region contributes to the observed radiation from the first micropinch, which typically emits a short burst of >3 keV radiation and has *L*-shell spectra characterized by broad spectral lines overlaying an intense continuum.

DOI: 10.1103/PhysRevE.70.026402 PACS number(s): 52.58.Lq, 52.70.La, 32.30.Rj, 32.70.Fw

I. INTRODUCTION

X pinches produce dense plasmas that reliably and efficiently emit radiation useful for x-ray imaging, as well as for studies of dense *z*-pinch plasma dynamics and x-ray spectroscopy of highly ionized, high-*Z* atoms [1–5]. *X*-pinches are produced by driving a large current through two or more fine wires that cross and touch in the middle, in the form of an "*X*." A dense *z*-pinch plasma is formed at the crossing point of the *X*-pinch wires that unstably implodes and emits one or some bursts of a few-keV x rays [6,7]. At currents of several hundred kiloamperes, these x-ray bursts last for several hundred picoseconds and originate from different "micropinches" within a 50–150 μm narrow-neck region in the imploding *z*-pinch [2].

The dynamics of *X*-pinch implosions have been extensively studied through both experimental x-ray backlighting [2] and magnetohydrodynamics (MHD) modeling [8]. Spectroscopic analysis can give further insight into the properties of the *X*-pinch plasma during the x-ray bursts. Spectroscopic analysis of *K*-shell line emission has been used to determine electron temperatures near 1 keV and ion densities from 10^{19} to 10^{24} cm^{-3} for Al [9] and Ti [7,9] *X*-pinch plasmas driven by 400 kA of current. More recently, *L*-shell spectroscopic models (first used in [10] and [11] to diagnose laser plasmas) have been applied to study time-integrated and time-gated Mo spectra from 1 MA *X*-pinch plasmas [6]. The present work uses the *L*-shell Mo model introduced in [6] to diagnose emission spectra from 470 kA Mo *X* pinches with 50 ps time resolution using a non-local thermodynamic equilibrium (NLTE) spectroscopic model.

Section II of this paper introduces the experimental configuration of the Mo *X* pinches and the diagnostic instrumentation. Section III describes the collisional-radiative model and density- and temperature-sensitive *L*-shell spectral features used for diagnostics. Comparisons of modeled spectra with streak camera spectra, which yield temperatures and densities as a function of time for three *X* pinches, are given in Sec. IV. In Sec. V, the results are summarized and a discussion of the implications of the spectroscopic analysis to *X*-pinch dynamics is given.

II. DESCRIPTION OF THE EXPERIMENT

The Mo *X* pinches were placed in the anode-cathode gap of the XP pulser [12], which generates a 470 kA, 100 ns FWHM current pulse. In all of the experiments presented here, two 17- or 20-μm two-wire Mo *X* pinches in parallel were used as the diode load. The *X* pinches each have a height of 15 mm and the wires are touch-crossed at the center. Schematic diagrams of the experimental setup for the *X*-pinch experiments are presented in Fig. 1.

A variety of diagnostics are fielded on a typical test. Detailed descriptions of each of the diagnostics shown in Fig. 1,

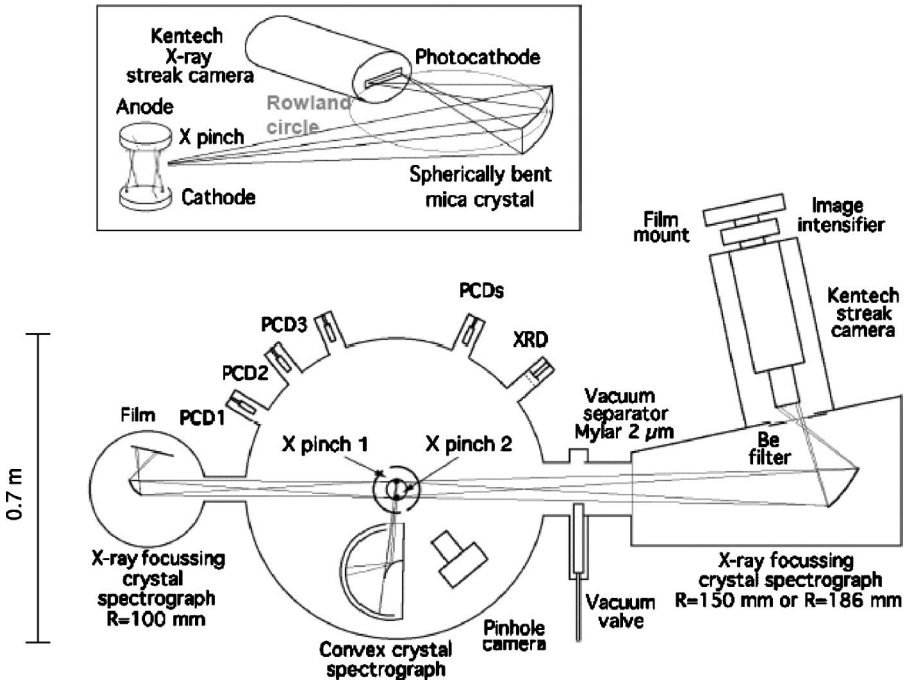

FIG. 1. Diagram depicting the diagnostic arrangement used for *X*-pinch experiments, including photoconducting diodes (PCDs) with different filters, x-ray diodes (XRDs), a time-integrated FSSR-1D spectrograph (at left) and the x-ray streak camera (to the right). Inset: Diagram depicting the FSSR-1D focusing spectrograph configuration used with the x-ray streak camera.

and the data obtained with them, have been published elsewhere [1,2,13,14]. The inset in Fig. 1 shows the arrangement of the streak camera with a spherically bent mica crystal in a focusing spectrograph with spatial resolution in one dimension (FSSR-1D). This configuration provides spectral resolution in one direction (in the Rowland circle plane) and one-dimensional spatial resolution in the orthogonal direction [2,4]. Radiation from a point source is spectrally dispersed along a narrow line.

The experiments used a Kentech low-magnification ($M=1.2$) x-ray streak camera [13] with a photocathode composed of CsI deposited on a 10 μm Be substrate. To protect the photocathode, a 50 μm Be filter was placed across the entrance to the streak camera vacuum chamber. The x-ray streak camera was used with nominal streak speeds of 4.9 and 15 mm/ns for total time windows of 8.2 and 2.7 ns and temporal resolutions of 20 and 7 ps, respectively. Streaked images were recorded directly on Kodak T-max 400 film placed in contact with the fiber-optic output. The x-ray streak camera was oriented so that its temporal direction was perpendicular to the spectral dispersion direction. The spectrograph configuration also has a spatial resolution of about 0.1 mm in the direction of spectral dispersion. X-ray bursts from the two *X* pinches can be distinguished, because the displacement of a small source in the plane of the Rowland Circle (see Fig. 1 inset) leads to a shift of the spectral lines. Further details of the imaging system and the calibration procedures are given in Refs. [3,4,7].

With two *X* pinches in parallel, each *X* pinch can be used to obtain radiographs of the other. In this way, images of the *X* pinch at times just before and just after the initial x-ray burst have been obtained. Radiographs showing the central portion of several Mo *X* pinches are shown in Fig. 2, along with plots of the Ne-like 3D line ($2s^2 2p^5 3d\ ^3D_1 - 2s^2 2p^6\ ^1S_0$) and continuum intensities obtained from the streak camera spectra that are analyzed below. Notice that two of the images in Fig. 2 are from the same pulse (1411). The one labeled $t=+0.3$ ns formed a micropinch 0.3 ns before the other, emitting its x-ray burst and producing the image of the other *X* pinch (labeled $t=-0.3$ ns). The latter emitted its x-ray burst 0.3 ns later, thereby providing the image of the first *X* pinch 0.3 ns after its x-ray burst.

The radiographs in Fig. 2 give a general picture of the plasma development around the time of the x-ray bursts. About 20 ns before the x-ray burst, a $\sim$300-μm-long *z* pinch that is $\sim$100 μm in diameter forms near the original wire crossing point [2]. This *z* pinch undergoes a radial implosion, developing sausage instabilities that lead to the formation of one or more narrow necks over a portion of the *z*-pinch column less than 1 ns before the first x-ray burst. This is illustrated by the radiograph in Fig. 2, obtained 0.6 ns before the maximum intensity of the first x-ray burst of that *X* pinch (pulse 1392), in which a plasma neck with a diameter around 10 μm can be seen. The ion density of this neck is estimated to be near 10^{22} cm^{-3} from the absorption of the imaging x rays [2]. There is little or no *L*-shell emission from the plasma at this time, indicating that its temperature is probably below about 100 eV. During the final $\sim$0.5 ns before the first x-ray burst, there is very rapid sausage instability development in the plasma neck and some portion of the neck implodes with a radial velocity estimated to be as high as 20–30 μm/ns. After this implosion, a gap opens up in the plasma column with ion densities near or below the $\sim 10^{19}$ cm^{-3} density level required for detectable x-ray absorption in a 30–50-μm-diam plasma. This phase of *X*-pinch dynamics is illustrated by the radiographs in Fig. 2 obtained 0.3 ns before and 0.3 ns after the peak of the x-ray bursts from those *X* pinches. The first x-ray bursts last for 0.3–0.4 ns and are known to come from micropinches that precede and are colocated with the gaps that appear within the plasma neck [2].

The lower portion of Fig. 2 shows x-ray intensities obtained from specific wavelengths in the spectra of the x-ray

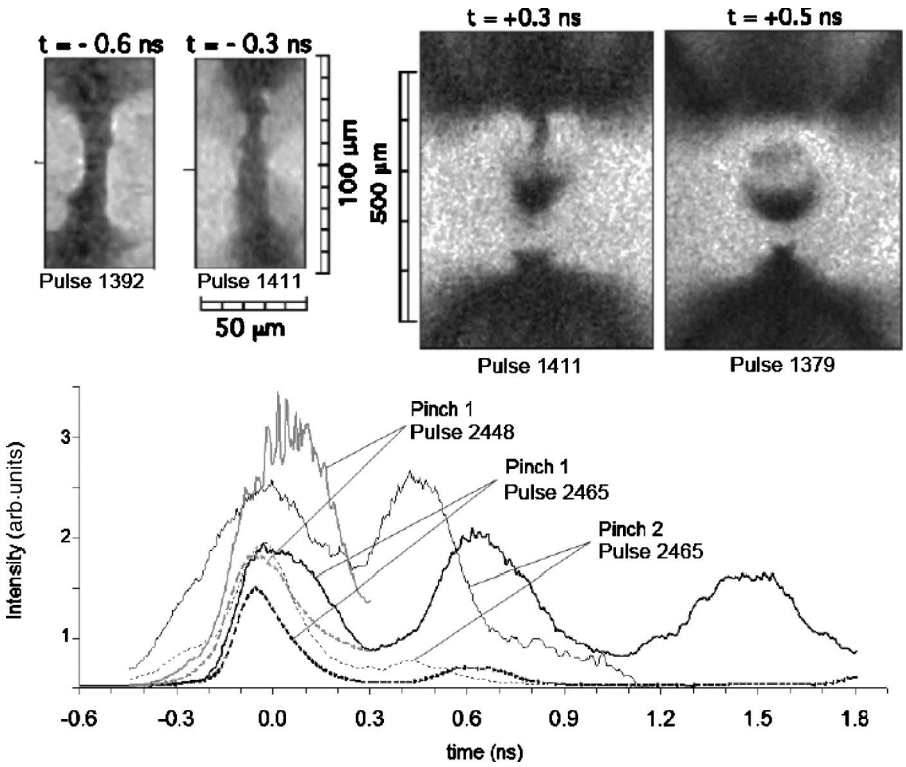

FIG. 2. Top: Radiographs of the central region of four *X* pinches, each made with two 17 -μm-diam Mo wires. The given times are relative to the maximum intensity of the first x-ray bursts from each of the imaged *X* pinches [2]. Bottom: Time histories of the Ne-like 3D line intensity (solid lines) and the continuum emission intensity between 4.75 and 4.79 Å (dashed lines) from one *X* pinch using 17 -μm-diam wires (pulse 2448) and two *X* pinches using 20-μm-diam wires (pulse 2465). The time zero in this figure is the moment of the maximum line-emission intensity from the first x-ray burst of each *X* pinch.

streaks that we analyze in Sec. IV. As shown by the dashed lines in Fig. 2, there is intense continuum emission in the first x-ray burst of a typical two-wire Mo *X* pinch that peaks 20–50 ps before the peak of the *L*-shell line radiation and persists for only about 200 ps (about half the duration of the *L*-shell line emission). After the initial x-ray burst, a gap forms in the plasma neck and the plasma appears to undergo an explosion centered at the location of the first x-ray burst, clearing the plasma out of the whole cross point region (at least to the 10^{19} cm^{-3} sensitivity limit of the x-ray imaging diagnostic) on a time scale of 2 ns with an explosion velocity estimated to be near 100 μm/ns [2]. It is common for there to be secondary *L*-shell x-ray bursts that occur within ~1 ns of the first one. Such bursts are observed to originate from different locations along the initial narrow plasma neck, have durations of 300–400 ps, and tend to have smaller continuum intensities than the first x-ray burst.

Measurements of energetic x-ray emission from the first x-ray burst have been made using photoconducting diodes (PCDs) filtered with 12.5 μm of Ti (which transmit x rays with energies of 3–5 and >8 keV). The energetic x rays measured by the PCD have diagnostic-system-limited pulses as short as 250 ps (FWHM). However, x-ray streak camera data obtained with the 12.5-μm Ti foil filter indicate that the energetic radiation is emitted with typical pulse durations of ~30 ps. Such short, energetic x-ray bursts occur sometime within the first 200 ps of x-ray emission that is dominated by the softer continuum shown in Fig. 2. Diffraction-limited imaging of fine metal meshes by Mo *X*-pinch radiation using the Ti filter indicates that the energetic radiation is emitted predominantly from a source that is ~1 μm in diameter [15]. By contrast, imaging without the Ti filter indicates that the *L*-shell emission originates from a substantially larger source that overlaps the location of the energetic (>3 keV) radiation source.

Apart from the ion density estimates obtained from radiographic imaging of *X* pinches and the source size estimates obtained from imaging studies, the conditions of Mo *X*-pinch plasmas during the x-ray bursts are not well known from direct measurements. The spectroscopic analysis of the plasma emission presented below gives a detailed picture of the evolution of the radiating plasma conditions.

III. DESCRIPTION OF THE *L*-SHELL Mo MODEL

Matching the predictions of collisional-radiative spectroscopic models to experimental observations of plasma emission is an effective and noninvasive plasma diagnostic method. Collisional-radiative models are based on a detailed description of the levels of ions in a plasma and the collisional and spontaneous rates that govern population transfer between them. In the present model, steady-state level populations are calculated using coupled collisional-radiative rate equations in the optically thin approximation. By varying the modeled plasma conditions, modeled spectra are fit to experimental spectra and used to infer the electron density (n_e) and electron temperature (T_e) of the emitting plasma.

The model used in this paper has been used previously to determine plasma conditions from time-integrated and time-gated *L*-shell Mo spectra obtained from *X* pinches driven by ~1 MA of current at the University of Nevada, Reno [6]. The model includes the ground states of all Mo ions and more than 6000 detailed levels, including singly excited levels up to $n=7$ for O- through Na-like Mo, singly excited levels up to $n=4$ for Mg-like Mo, and doubly excited levels up to $n=4$ for Na- and Mg-like Mo. The levels are fully coupled by radiative decay and radiative recombination, and by collisional excitation, ionization, Auger decay, and their

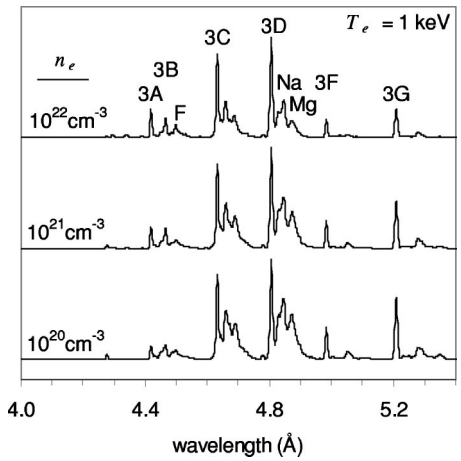

FIG. 3. Modeled *L*-shell Mo spectra with $T_e=1$ keV and the labeled electron densities. Ne-like Mo lines (3A–3G) and F-, Na-, and Mg-like Mo features are labeled in the top spectrum.

reverse rates. Modeled spectra are constructed using Voigt line profiles, the width and shape of which are free parameters. Continuum emission from radiative recombination and bremsstrahlung processes are calculated self-consistently within the spectroscopic model. Further details of the model are given in Ref. [6].

Figure 3 shows the electron-density dependence of modeled *L*-shell Mo spectra. The Ne-like Mo lines are labeled in the top spectrum of Fig. 3 with their common designations [10]: 3A and 3B are $3p$-$2s$ transitions, 3C and 3D are $3d$-$2p$ transitions, and 3F and 3G are $3s$-$2p$ transitions. Diagnostically important features from F-, Na-, and Mg-like Mo are also labeled. Figure 3 shows that increasing the electron density from 10^{20} cm^{-3} to 10^{22} cm^{-3} increases the charge state balance of the plasma, shifting emission from Na- and Mg-like Mo towards F-like Mo. This effect is similar to that of increasing the electron temperature, but is distinguishable from the temperature dependence because increasing the electron density also decreases the intensities of the Ne-like 3F and 3G lines relative to the other Ne-like lines. The intensities of the 3F and 3G lines are amplified at low densities by radiative cascades from higher levels. As the electron density increases, these cascades are disrupted by collisions and the 3F and 3G line intensities decrease. The ratio 3B/3F is a good density diagnostic, because it increases monotonically with increasing electron density and is relatively insensitive to the electron temperature.

The ratio 3B/3F can be extracted from the given experimental data with a precision of 10–20 % by integrating over the measured intensity of the emission lines. This precision includes uncertainties caused by noise in the experimental intensities, plausible variations in the estimated continuum emission (discussed below), and the effects of nonuniformity in the streak camera response across the spectral range. With this experimental precision, electron densities can be inferred from the 3B/3F ratio with confidence to within a factor of 2. The electron temperature can be determined to within about 10% by fitting the relative intensities of the Ne-like Mo lines to Na- and Mg-like satellite features. The temperature uncertainty estimate includes uncertainties derived both from experimental precision and from the density dependence of temperature within the stated density range.

It is not immediately obvious that the plasma is in steady-state equilibrium within ~50 ps time frames and optically thin everywhere. We have therefore performed calculations to verify that steady-state and optically thin spectra are adequate representations of the plasma emission. First, we have used the diagnosed steady-state conditions to drive a fully time-dependent model and have found that the time-dependent spectra have line intensities very close to those determined in the steady state. Second, we have included the effects of opacity using a full solution of the radiative transfer equation with slab geometry and self-consistent level populations for the extreme case of a 10 μm plasma with an electron density of 10^{23} cm^{-3}, and have found minimal effects on line intensities and widths. We are therefore convinced that steady-state and optically thin spectra can be reliably used to determine the plasma temperatures and densities using the straightforward diagnostic procedure described above.

IV. RESULTS

A. Comparison of experimental and modeled *L*-shell Mo spectra

Spectra from two experimental tests, each with two Mo *X* pinches in parallel, have been analyzed. Each of the *X* pinches in both tests emitted two to four x-ray bursts that were captured on the streak camera film. The spectra from the two *X* pinches in each test are distinguishable on the streak camera film by the different dispersions of the spectral lines due to the spatial separation of the *X* pinches. The first x-ray burst from each *X* pinch is typically characterized by broad spectral lines and an intense continuum, while later bursts have narrower lines and smaller continuum intensities.

Figure 4(a) shows the streak camera image of *L*-shell emission from two 20-μm-wire *X* pinches (pulse 2465). Darker regions on the streak camera image indicate more emission (in proportion to the photon number incident on the streak camera). The first three x-ray bursts were all emitted from the first *X* pinch. Spectral intensity profiles ("lineouts") integrated over 54 ps near the maximum intensity of each of the three bursts are given by the gray lines in Fig. 4(b). The best-fit modeled spectra are given by the overlaid thin black lines and are labeled with the modeled T_e and n_e. Continuum intensities subtracted from the experimental spectra to obtain the best-fit modeled spectra are shown by dashed lines.

The bottom spectrum in Fig. 4(b) was taken from the first x-ray burst of the first *X* pinch. It has intense continuum emission and broad spectral lines. The relative intensities of the spectral lines and features are fit well by a modeled spectrum with $T_e=1$ keV and $n_e=1.5\times10^{22}$ cm^{-3}. This fit requires significant artificial broadening of the modeled spectral lines. (Neither the bulk-plasma motion nor the collisional broadening included in the model can fully account for the observed broadening.) Spectra from the two subsequent bursts of the first *X* pinch (0.65 and 1.45 ns after the initial burst) have weaker continuum emission and narrower lines. Both are fit well by modeled spectra with electron tempera-

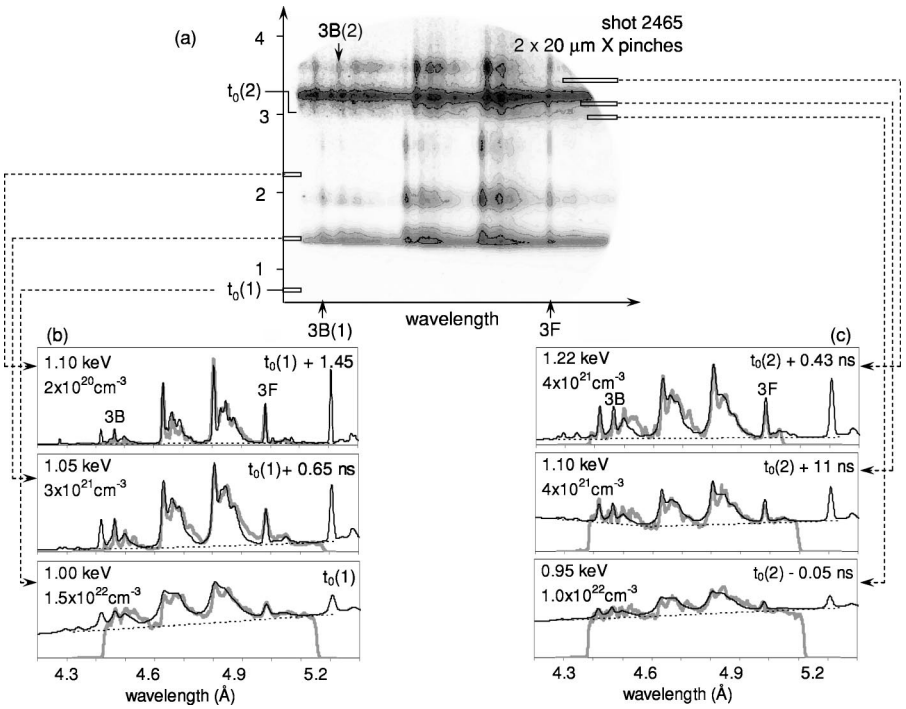

FIG. 4. (a) Streak-camera image from two 20-μm Mo wire *X* pinches (pulse 2465). (b) Lineouts over 54 ps (gray lines) at the maximum intensities of the x-ray bursts from the first micropinch overlaid with modeled spectra at the given conditions (thin black lines). (c) Lineouts over 54 ps (gray lines) near the maximum intensities of the two x-ray bursts from the second micropinch overlaid with modeled spectra at the given conditions (thin black lines). In (b) and (c), the continuum that was subtracted from the experimental spectra before fitting the model spectra to the data is given by dashed lines.

tures near 1 keV and much smaller densities than the first burst, with little or no artificial broadening beyond the nominal instrumental broadening.

Figure 4(c) gives experimental spectra obtained from 54 -ps lineouts near the maximum intensities of the two captured x-ray bursts from the second *X* pinch of pulse 2465 overlaid with modeled spectra. The bottom spectrum in Fig. 4(c), taken about 50 ps before the maximum intensity of the first burst, has intense continuum emission and broad spectral lines. It is fit well by a modeled spectrum with $T_e = 0.95$ keV and $n_e = 10^{22}$ cm^{-3}. The middle spectrum, taken 110 ps after the maximum intensity of the first burst, already has much smaller continuum intensity and narrower spectral lines than the spectrum from 50 ps before the first x-ray burst. It is fit well by a modeled spectrum with $T_e = 1.1$ keV and $n_e = 4 \times 10^{21}$ cm^{-3}. The top spectrum in Fig. 4(c), taken at the maximum intensity of the second burst, is very similar to the spectrum from the second burst of the first *X* pinch shown in Fig. 4(b).

Figure 5(a) shows the streak camera image of *L*-shell emission from two 17-μm wire *X* pinches (pulse 2448). Experimental and modeled spectra from the first x-ray burst are given in Fig. 5(b). The second x-ray burst in the streak camera image in Fig. 5 includes emission from the second *X* pinch; subsequent bursts from the two *X* pinches are interlaced. Although most spectral lines from the two *X* pinches are shifted away from each other and can be distinguished on the streak camera image, the 3F lines coincide. Because of this coincidence and the close temporal spacing of the x-ray bursts, the electron density for the later bursts cannot be diagnosed with confidence and only the first x-ray burst from the first *X* pinch has been analyzed. The spectra and plasma parameters from the first x-ray burst are very similar to those of the first burst of the two 20-μm *X* pinches, with the relative continuum intensity decreasing and the *L*-shell lines narrowing over the ~0.4 ns duration of the burst.

There are strong similarities among the three diagnosed *X* pinches. In all three cases, the first x-ray bursts have the broadest lines, the largest continuum intensities, and are di-

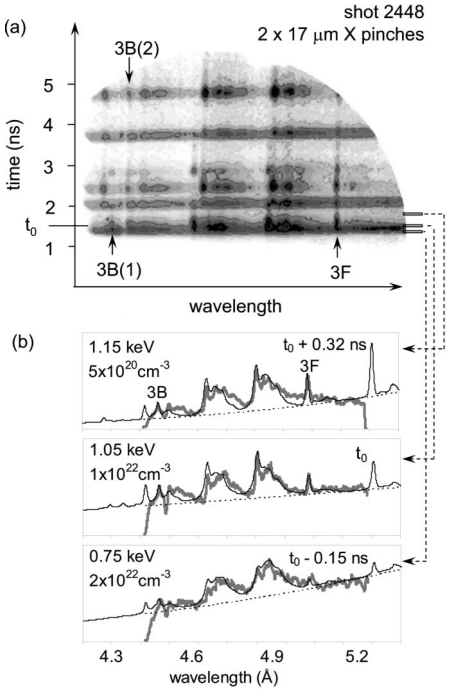

FIG. 5. (a) Streak-camera image of *L*-shell emission from two 17-μm Mo wire *X* pinches (pulse 2448). (b) Lineouts integrated over 43 ps (gray lines) before, during, and after the intensity maximum of the first x-ray burst in the image overlaid with modeled spectra (thin black lines) at the labeled conditions. The continuum that was subtracted from the experimental spectra before fitting the model spectra to the data is also shown (dashed lines).

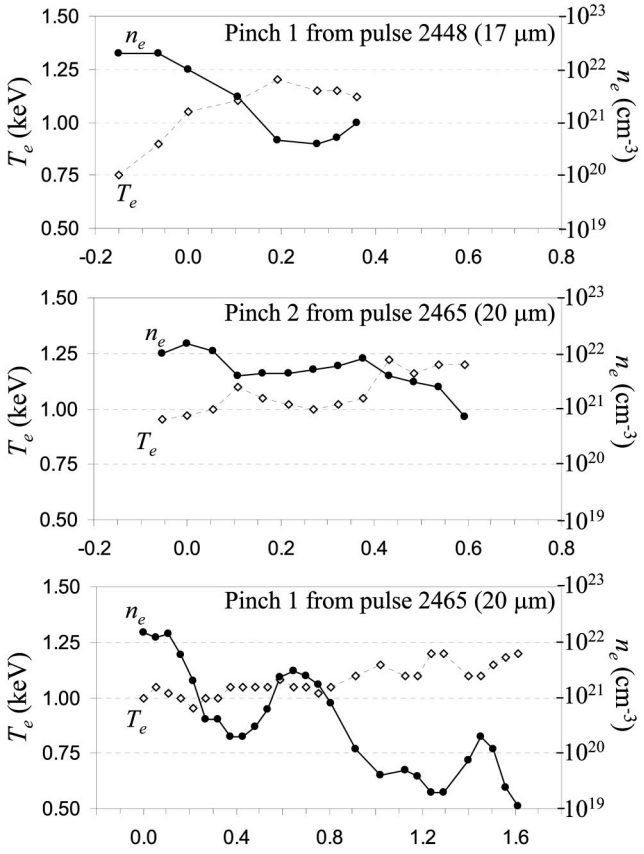

FIG. 6. Electron temperatures (open circles) and densities (solid circles) determined from the spectra of three *X* pinches as a function of time.

agnosed to have $n_e \sim 10^{22}$ cm^{-3} and $T_e \sim 1$ keV. However, while the continuum intensity in both the first 20-μm *X* pinch and the 17-μm *X* pinch increases monotonically with the wavelength (with a slope corresponding to a simple model of continuum emission with intensity proportional to $\exp(-h\nu/T_c)$ with $h\nu$ the photon energy and $T_c \sim 1$ keV), there is a ~180 ps period during which the continuum emission from the second 20-μm *X* pinch decreases from 4.3 to 4.6 Å. [This period is from ~35 ps before the maximum intensity of the first burst to ~145 ps afterwards: see the middle spectrum in Fig. 4(c).] It is unlikely that this feature is due to radiative recombination, which is generally at least 100 times smaller than the line intensities in the present model. A possible explanation for the anomalously intense continuum emission is presented in Sec. V below.

B. Plasma conditions during the x-ray bursts

The plasma parameters determined from streak camera *L*-shell spectra averaged over ~50 ps from the three *X* pinches are given as a function of time in Fig. 6. The first bursts from each of the *X* pinches have inferred peak electron densities above 10^{22} cm^{-3} and temperatures from 0.75 to 1.05 keV. The peak electron densities are diagnosed to occur within ~100 ps of the peak *L*-shell line intensities (as given in Fig. 2) and persist for about 200 ps. As the line intensities decrease over ~200 ps, the electron densities decrease by factors of 2–10 and the electron temperatures increase by a few hundred eV. The electron density decreases most markedly for the first 20-μm Mo wire *X* pinch of pulse 2465 and least for the second *X* pinch of the same pulse. The second x-ray bursts from both 20-μm *X* pinches have densities between 10^{21} and 10^{22} cm^{-3}, and temperatures between 1.1 and 1.25 keV. The third x-ray burst from the first 20-μm *X* pinch has a maximum density of only 2×10^{20} cm^{-3} and a temperature near 1.2 keV. The dimensions of the line-emitting regions of the first 20-μm *X* pinch can be estimated using the diagnosed plasma parameters. Mo *X* pinches typically emit ~100 mJ of >1.5 keV radiation. On the assumptions that all of the >1.5 keV x rays from the first 20-μm *X* pinch were emitted in the three observed bursts, and that the intensity of the total x-ray emission follows the energy-integrated intensity of the emission region captured by the streak camera, a normalized time history of the experimental energy emission rate in *L*-shell lines can be obtained. The radiative power can also be extracted from the model for a given T_e and n_e by summing over all spectral lines with energies greater than 1.5 keV. This modeled energy emission rate can be used to determine the number of ions required to produce the experimental rates: 10^{12} ions in the first x-ray burst and 10^{13}–10^{14} ions in the later x-ray bursts. The ion density can be obtained from the electron density and the average charge state (assuming a neutral plasma) and used with the required number of emitting ions to determine the spatial extent of the line-emitting plasma region.

In this way, the *L*-shell line-emitting region is estimated to be very near 10 μm in size during the first x-ray burst. The explosion velocity of the plasma during the first x-ray burst is on the order of 100 μm/ns—a bulk plasma motion that may account for the observed line broadening in the later half of the first x-ray burst, though not for the line broadening in the first half of the first x-ray burst. The line-emitting region during the second x-ray burst is estimated to be ~50 μm, increasing to at least 100 μm during the third x-ray burst. After the third x-ray burst, the line-emitting region increases up to near 1 mm, indicating that the entire plasma in the vicinity of the original *X*-pinch wire crossing point contributes to the line emission. Since individual x-ray bursts from similar *X* pinches have been determined to come from slightly different locations along the *z*-pinch necks shown in the images in Fig. 2 [2], the later x-ray bursts are not simply a result of repinching of the plasma at the same location to a larger minimum diameter and lower density.

V. SUMMARY AND DISCUSSION

L-shell spectra from three Mo *X* pinches have been diagnosed with a NLTE collisional-radiative kinetics model. The first x-ray bursts from each of the three pinches are characterized experimentally by broad spectral lines and significant continuum emission. The *L*-shell emission from those first bursts lasts for 0.3–0.4 ns. Averaged over ~50 ps near the maximum intensities of the first x-ray bursts, the *L*-shell

spectra indicate electron densities near 10^{22} cm^{-3} and electron temperatures from 0.75 to 1 keV. The size of the line-emitting region of the first x-ray burst is estimated to be around 10 μm. Later x-ray bursts have similar durations, narrower spectral lines, and less continuum emission. The *L*-shell spectra from the later bursts are indicative of electron densities around 10^{20}–10^{21} cm^{-3} and temperatures slightly above 1 keV; emission from the later bursts may originate from a plasma region that extends over the entire crossing-point region of the *X*-pinch wires.

The collisional-radiative equilibrium model is able to reproduce the relative intensities of the experimental *L*-shell lines throughout the emitting period of the *X* pinches quite well. In addition, the inferred conditions of the Mo *X*-pinch plasma during the x-ray bursts are generally consistent with the nonspectroscopic diagnostics noted in Sec. II. The magnetic energy within a millimeter of a few-μm-diameter micropinch carrying 225 kA is sufficient to provide the energy contained in, and radiated by, the *X* pinch (i.e., the ionization energy plus 1 keV per electron of thermal energy for 10^{13}–10^{14} Mg- to Ne-like Mo ions plus a few tens of J of total radiation). The dimension of the *L*-shell line emission region (tens or hundreds of microns) and its duration (0.3–0.4 ns) are consistent with the explosive pinch plasma expansion immediately after micropinch formation and peak x-ray burst emission (i.e., the gaps in the two images obtained after x-ray burst emission in Fig. 2).

There is evidence that a substructure exists in the initial *X*-pinch implosion that cannot be diagnosed using the *L*-shell line emission alone: First, a ~30 ps burst (a duration shorter than the lineout width used for the *L*-shell spectra) of >3 keV x rays is commonly observed from similar Mo *X*-pinch tests and is known to come from a ~1-μm plasma region [13]. Next, radiographic absorption data from similar *X*-pinch tests indicate that the ion density is around 10^{22} cm^{-3} in the 10-μm-diam plasma neck 0.6 ns before the first x-ray burst (Fig. 2, leftmost image). Even if 50–70 % of the ions are lost during the implosion of this 10-μm-diam neck to a ~1-μm plasma region, ion densities during the first x-ray burst should be near 10^{23} cm^{-3}, implying electron densities near 10^{24} cm^{-3} for 10 to 30 times ionized Mo. However, the *L*-shell line emission indicates peak electron densities no larger than a few times 10^{22} cm^{-3} in the first x-ray burst. Finally, the *L*-shell Mo emission model presented above does not account for the significant line broadening and intense continuum emission that are observed in the first ~200 ps of the initial x-ray burst.

We tentatively propose the following picture of the *X*-pinch dynamics during the first x-ray burst to account for the >3 keV x-ray emission, the anomalous line broadening, and the intense continuum emission: Mo ions in the initial ~300-μm-long *z*-pinch plasma that forms at the wire cross point are only a few times ionized. As the plasma implodes due to the high current, the Mo ions gain directed energy. The ~30 ps burst of >3 keV x rays occurs at the point of maximum compression in this implosion, at which time the source is ~1 μm in size and has an electron density near 10^{23} cm^{-3}. This small, dense source begins to explode and ionize rapidly over the next ~100 ps, as *L*-shell line emission from Ne-like and nearby ions emerges from the continuum. The anomalous continuum intensity and line broadening in the *L*-shell spectra during the first ~100 ps of the first x-ray burst may be due to inner-shell excitation of 10 to 30 times ionized Mo during this rapid ionization phase. Observation of significant line broadening and intense "quasi-continuum" emission in spectra from an electron-beam ion trap with $n_e \sim 10^{12}$ cm^{-3} [16] offers experimental evidence that such effects can be present even at very small electron densities. The quasicontinuum is thought to be caused by line emission from a multitude of weak transitions from several charge states, and can be much more intense than the normal continuum included in the present model. Quasicontinuous spectral features have also been observed in high-density laser plasma experiments [17]. As the plasma explodes, line emission from Ne-like Mo and nearby ions overtakes the strong quasicontinuum emission and persists for several hundred ps after stagnation. The high electron temperature is maintained by dissipation of magnetic energy in the exploding plasma as the current moves out to plasma at a larger radius. We estimate that this picture of the first x-ray burst can account for both the observed continuum intensity and the measured energy emitted in the >3 keV x-ray burst.

The later x-ray bursts are known to be emitted by secondary micropinches that form in different locations along the plasma neck. The reduced continuum intensity and the dominance of *L*-shell radiation at the peak emission intensity of the later bursts suggest that the secondary micropinches are already ionized to the *L* shell when they reach peak density. The spectroscopic results also indicate that the *L*-shell lines from the later x-ray bursts are emitted from a plasma region that has a lower density and a larger size (up to hundreds of μm) than the initial burst. This suggests that the line emission is radiated from the entire crossing-point plasma region, consistent with the two positive-time images in Fig. 2.

Finally, we note that suprathermal or "hot" electrons may be present in the form of current-carrying beams that are accelerated across the gap in the plasma neck and deposit their energy in the dense plasmas at the ends of the *z* pinch as it explodes (see the right-most panel in Fig. 2). Hot electron fractions of a few percent have been inferred from *L*-shell spectra of Mo *X* pinches driven by 1 MA of current at the Nevada Terawatt Facility using the present model [6], and much smaller hot electron fractions have been inferred from *K*-shell spectra of Al *X* pinches from the XP pulser [9]. The signatures of hot electrons in *L*-shell spectra include spread-out charge state balances, amplified intensities of lines fed by radiative cascades, and a distortion of satellite line structures [18]. Although the present experimental spectra are well described by modeled spectra at a single temperature, they can also be described using slightly higher electron densities, lower electron temperatures, and some fraction of hot electrons. However, the experimental charge state balances and spectral resolution are such that the spectra cannot be used to unambiguously infer the presence of hot electrons. The presence and spatial extent of hot electrons in these Mo *X* pinches can potentially be determined with space-resolved $K\alpha$ emission measurements [4]. The directionality and energy of electron beams that might be present in the *X*-pinch plasmas could be determined using spectropolarimetry [19].

ACKNOWLEDGMENTS

The authors thank Peter Beiersdorfer for helpful discussions regarding quasicontinuum and line broadening. We also thank Kevin Fournier and Ulyana Safronova for providing data used in the calculations. This work was supported by the DOE Cooperative Agreement DE-F03-02NA00057, DOE Grant No. DE-FG02-98-ER54496, and Sandia National Laboratories under Contract No. BD 9356. The work of A.S. and S.H. was also supported by the DOE-NNSA/NV Cooperative Agreement DE-FC08-01NV14050.

[1] T. A. Shelkovenko, D. B. Sinars, S. A. Pikuz, K. M. Chandler, and D. A. Hammer, Rev. Sci. Instrum. **72**, 667 (2001).
[2] T. A. Shelkovenko, D. B. Sinars, S. A. Pikuz, and D. A. Hammer, Phys. Plasmas **8**, 1305 (2001).
[3] S. A. Pikuz, T. A. Shelkovenko, D. B. Sinars, D. A. Hammer, S. V. Lebedev, S. N. Bland, I. Yu. Skobelev, J. A. Abdallah, C. J. Fontes, and H. L. Zhang, J. Quant. Spectrosc. Radiat. Transf. **71**, 581 (2001).
[4] T. A. Shelkovenko, S. A. Pikuz, D. B. Sinars, K. M. Chandler, and D. A. Hammer, Phys. Plasmas **9**, 2165 (2002).
[5] S. A. Pikuz, D. B. Sinars, T. A. Shelkovenko, K. M. Chandler, D. A. Hammer, I. Yu. Skobelev, G. V. Ivanenkov, and W. Stepniewski, Phys. Rev. Lett. **89**, 035003 (2002).
[6] A. S. Shlyaptseva, S. B. Hansen, V. L. Kantsyrev, D. A. Fedin, N. Ouart, K. B. Fournier, and U. I. Safronova, Phys. Rev. E **67**, 026409 (2003).
[7] D. B. Sinars, S. A. Pikuz, T. A. Shelkovenko, K. M. Chandler, D. A. Hammer, and J. P. Apruzese, J. Quant. Spectrosc. Radiat. Transf. **78**, 61 (2003).
[8] G. V. Ivanenkov and W. Stepniewski, Plasma Phys. Rep. **28**, 814 (2002).
[9] J. Abdallah, Jr., A. Ya. Faenov, D. A. Hammer, S. A. Pikuz, G. Csanak, and R. E. H. Clark, Phys. Scr. **53**, 705 (1996).
[10] J. Bailey, R. E. Stewart, J. D. Kilkenny, R. S. Walling, T. Phillips, R. J. Fortner, and R. W. Lee, J. Phys. B **19**, 2639 (1986).
[11] W. H. Goldstein, R. S. Walling, J. Bailey, M. H. Chen, R. Fortner, M. Klapisch, T. Phillips, and R. E. Stewart, Phys. Rev. Lett. **58**, 2300 (1987).
[12] D. H. Kalantar, Ph.D. dissertation, Cornell University, 1993.
[13] D. B. Sinars, Ph.D. dissertation, Cornell University, 2001.
[14] D. B. Sinars, Rev. Sci. Instrum. **72**, 2948 (2001).
[15] B. M. Song, S. A. Pikuz, T. A. Shelkovenko, D. A. Hammer, K. M. Chandler, and M. D. Mitchell, submitted to Appl. Opt.
[16] P. Beiersdorfer, J. K. Lepson, G. V. Brown, S. B. Utter, S. M. Kahn, D. A. Liedahl, and C. W. Mauche, Astrophys. J. Lett. **519**, L185 (1999).
[17] A. Ya. Faenov, A. I. Magunov, T. A. Pikuz, and I. Yu. Skobelev, Phys. Scr. **T80**, 536 (1999).
[18] S. B. Hansen, Ph.D. dissertation, University of Nevada, Reno, 2003.
[19] A. S. Shlyaptseva, D. A. Fedin, S. M. Hamasha, S. B. Hansen, C. Harris, V. L. Kantsyrev, P. Neill, N. Ouart, P. Beiersdorfer, and U. I. Safronova, Rev. Sci. Instrum. **74**, 1947 (2003).